KECK-NIRSPEC INFRARED OH LINES: OXYGEN ABUNDANCES IN METAL-POOR STARS DOWN TO [Fe/H] = −2.9 [1]

Jorge Meléndez and Beatriz Barbuy
Universidade de São Paulo, IAG, Dept. de Astronomia, CP 3386, São Paulo 01060-970, Brazil
E-mail: jorge@astro.iag.usp.br, barbuy@astro.iag.usp.br

ABSTRACT

Infrared OH lines at 1.5 - 1.7 μm in the H band were obtained with the NIRSPEC high-resolution spectrograph at the 10m Keck Telescope for a sample of seven metal-poor stars. Detailed analyses have been carried out, based on optical high-resolution data obtained with the FEROS spectrograph at ESO. Stellar parameters were derived by adopting infrared flux method effective temperatures, trigonometric and/or evolutionary gravities and metallicities from Fe II lines. We obtain that the sample stars with metallicities [Fe/H] < -2.2 show a mean oxygen abundance [O/Fe] ≈ 0.54, for a solar oxygen abundance of ϵ(O) = $\approx$ 8.87, or [O/Fe] ≈ 0.64 if ϵ(O) = 8.77 is assumed.

1. Introduction

Oxygen abundances in metal-poor stars are a key information for understanding the early phases of Galactic chemical evolution. Very few data on oxygen abundances are available for stars with metallicities around [Fe/H] $\approx$ -3.0, and results obtained from different lines are often discrepant.

The infrared (IR) $X^2\Pi$ vibration-rotation transitions of OH lines in the H band were first used in halo stars by Balachandran & Carney (1996) for the dwarf HD 103095, having derived [Fe/H] $= -1.22$ and [O/Fe] $= 0.29$. Balachandran et al. (2001, 2002) and Meléndez et al. (2001) presented new oxygen abundance determinations in metal-poor stars, from OH lines in the H band. Their [O/Fe] values tend to show agreement with those derived from [OI] lines in the metallicity range -1.0 $\lesssim$ [Fe/H] $\lesssim$ -2.5; three among the four analyzed stars of lower metallicities give higher values.

The oxygen abundance determination using IR OH lines may solve the problem of disagreement between the values obtained from different oxygen abundance indicators. The IR OH lines in the H band of the first overtone have measurable intensities down to [Fe/H] $\sim$ -3.0 for giants with effective temperatures $T_{\rm eff} \sim 4500$ K, and [Fe/H] $\sim$ -3.5 for $T_{\rm eff} \sim 4300$ K, whereas for dwarfs the lines are stronger, and with effective temperatures $T_{\rm eff} \sim 4500$ K, stars of [Fe/H] $\sim$ -3.5 could be measured. Otherwise only the fundamental transition lines at 3.5 μm, in the L band, are measurable. (The difficulty with these latter lines comes, however, from the thermal background and lower sensitivity of the instruments.) The relative intensity of the OH lines in the L and H bands can be seen in Hinkle et al. (1995) for Arcturus, and for the Sun in Livingston & Wallace (1991), in which only the L-band lines are seen.

IR vibration-rotation OH lines tend to form in LTE, whereas the electronic transition UV lines tend to form in non-LTE (Hinkle & Lambert 1975). Non-LTE effects in the formation of OH will affect both sets of lines, according to Asplund & García-Pérez (2001, hereafter AGP01).

In the present work we use IR OH lines in the region 1.5 - 1.7 μm in order to derive oxygen-to-iron ratios for a sample of seven metal-poor stars, most of them in the metallicity range -3.0 $<$ [Fe/H] $<$ -2.0.

[1] Observations carried out with the Keck Telescope within the Gemini-Keck agreement, and at the European Southern Observatory

In Sect. 2 the observations are presented. In Sect. 3 the detailed analyses are described. In Sect. 4 the results from IR OH lines are discussed, and in Sect. 5 conclusions are drawn.

2. Observations

2.1. Data Acquisition and Reduction

High-resolution infrared spectra were obtained from images taken at the 10m Keck Telescope, using the NIRSPEC spectrograph (McLean et al. 1998). FWHM resolutions of 37,000 were achieved with the échelle grating, with a 2-pixel slit width. The detector is an Aladdin 1024x1024 InSb array, covering essentially all the H band in the range 1.5-1.7 μm, apart from small gaps (0.008 μm) between the orders.

Each star was observed at two slit positions with the same integration time. A final flatfield and a dark image were prepared by the Gemini/Keck team.

These infrared data were reduced using IRAF. The sky background was eliminated by subtracting the exposures from the sky obtained in the first/second exposures at the same position in the detector. Flat-field and dark corrections were applied. The orders were extracted with the task APALL. The wavelength calibration was carried out using the provided Ar-Ne-Xe-Kr lamp spectrum. Signal-to-noise ratios (S/Ns) of $\approx$ 150-400 were estimated from continuum regions and reported in Table 1.

Optical spectra were obtained at the 1.52m telescope at ESO, La Silla, using the Fiber-fed Extended Range Optical Spectrograph (FEROS) (Kaufer et al. 2000). The total spectrum coverage is 356-920 nm with a resolving power of 48,000. Two fibers, with entrance aperture of 2.7 arcsec, simultaneously recorded starlight and sky background. The detector is a back-illuminated CCD with 2948$\times$4096 pixels of 15 μm size. Sample stars were reduced through a special pipeline package for reductions (DRS) of FEROS data, in a MIDAS environment. The data reduction proceeded with subtraction of bias and scattered light in the CCD, orders extraction, flat-fielding, and wavelength calibration with a ThAr calibration frame.

The log of observations is given in Table 1.

3. DETAILED ANALYSIS

The sample consists of six very metal poor giants and one dwarf of intermediate metallicity.

3.1. Effective Temperatures

Colors available in the literature were taken from the following sources: J, H and K in the TCS (Telescopio Carlos Sánchez) system from Alonso, Arribas & Martínez-Roger (1994, 1998); Strömgren $ubvy$-β from the Catalogue by Hauck & Mermilliod (1998); $V-R$ (Cousins) from McWilliam et al. (1995); and $V-R$, J, H and K from the General Catalogue of Photometric Data (Mermilliod, Mermilliod & Hauck 1997). Transformations between different photometric systems were calculated using relations given by Bessell (1979), Bessell & Brett (1988) and Alonso et al. (1994, 1998).

The reddening values of most stars, estimated by using the maps of reddening by Burstein & Heiles (1982), were taken from Anthony-Twarog & Twarog (1994). Otherwise, they were determined using maps by Arenou et al. (1992) and several high-Galactic latitude surveys, as implemented in a FORTRAN code by Hakkila et al. (1997). The reddening $E(B-V)$ and the dereddened colors are given in Table 2. Distances were determined from *Hipparcos* parallaxes (Perryman et al. 1997) for 2 stars; otherwise we used the same procedure as Anthony-Twarog & Twarog (1994).

Effective temperatures $T_{\rm eff}$ determined using the $b-y$, $V-R$, $V-K$ and $J-K$ calibrations of Alonso, Arribas & Martínez-Roger (1996a, 1999a, hereafter AAM99a) are given in Table 3. In this table are also shown infrared flux method (IRFM, column 7) temperatures, as determined by Alonso, Arribas & Martínez-Roger (1996b, 1999b, hereafter AAM99b). The mean of the IRFM calibrations (AAM99a,AAM99b), which are essentially the same as the IRFM determinations by AAM99b, are shown in column 8 of Table 3. These mean values were checked against excitation equilibrium of Fe I lines. The temperatures based on excitation equilibrium of Fe I are in the mean 18 K hotter than the mean of IRFM temperatures. The small difference between Fe I temperatures and the IRFM temperatures is an indication that non-LTE effects are minor (Tomkin & Lambert 1999).

3.2. Gravities

Nissen et al. (1997) and Allende Prieto et al. (1999) have shown that LTE spectroscopic gravities are lower than trigonometric gravities derived from *Hipparcos* parallaxes in metal-poor stars. For this reason, *Hipparcos* parallaxes π were used to derive trigonometric gravities, when parallax values were available, which was the case for two stars. For the others, we derived the gravity by estimating their absolute magnitudes in colour-magnitude diagrams, using the calibrations by Norris et al. (1985). These gravities are given in Table 4. The same method was also applied to the stars of Meléndez et al. (2001), since their parallaxes, and consequently their gravities, had large uncertainties. The revised evolutionary gravities log g and oxygen abundances are presented in Table 5.

Note that ionization equilibrium should not be used, given that Fe I lines show non-LTE effects (Thévenin & Idiart 1999).

3.3. Metallicities

Equivalent widths of Fe I and Fe II lines for 5 stars (except for HD 134440 and HD 122956)were measured on high-resolution spectra obtained with the FEROS spectrograph at ESO. For HD 134440, we adopted equivalent widths from Ryan & Deliyannis (1998), Tomkin & Lambert (1999), and Fulbright (2000), and for HD 122956, those by Sneden et al. (1991) and Fulbright (2000).

We compare the equivalent widths measured from the FEROS spectra with those from the Lick Observatory. The comparison of 20 lines from FEROS with those from the Hamilton/Lick data by Sneden et al. (1991) gives δ(EW) = EW$_{ESO}$ - EW$_{Lick}$ = +0.1±0.7 mÅ (σ = 3.2 mÅ), and another 40 lines with Fulbright (2000) gives δ(EW) = EW$_{ESO}$ - EW$_{Lick}$ = +0.8±0.5 mÅ (σ = 2.9 mÅ).

MARCS model atmospheres by Bell et al. (1976) and Gustafsson et al. (1975) were used for the calculations of curves of growth and spectrum synthesis.

The adopted oscillator strengths for the optical iron lines are from Nave et al. (1994), which correspond in most cases to gf-values from O'Brian et al. (1991), and in cases where the lines are not given in O'Brian et al., the values are from the National Institute of Standards & Technology (Fuhr, Martin, & Wiese 1988) and a few other references. The mean difference in log gf values between O'Brian et al.(1991) and the NIST database is of δlog gf (O'Brian et al - NIST) = 0.02.

On the other hand, gf-values of Fe II lines show a larger variation in the literature. We have adopted theoretical gf-values by Biémont et al. (1991), calibrated with experimental data as follows: lifetimes of upper levels from Schnabel et al. (1999), Schnabel & Kock (2001), Guo et al. (1992), Hannaford et al. (1992), and Biémont et al. (1991) and branching ratios by Heise & Kock (1990), Pauls et al. (1990), and Kroll & Kock (1987) are adopted, and gf-values are computed. These values are gathered in multiplets, and corrections are applied from comparisons between the theoretical and laboratory values.

Curves of growth and abundances from equivalent widths of Fe I and Fe II were computed using the codes RENOIR and ABON by M. Spite. Microturbulence velocities v_t were obtained from curves of growth of Fe I, and these values were checked by requiring no dependence of [Fe/H] against reduced equivalent width.

In Table 6 are given the Fe abundances derived from IRFM effective temperatures, trigonometric or evolutionary gravities, and curves of growth based on optical Fe II lines, and literature parameters for comparison purposes.

3.4. Oxygen Abundances

The oxygen abundances were determined from fits of synthetic spectra to the sample spectra. The LTE code for spectrum synthesis described in Cayrel et al. (1991) was employed for the calculations. In all cases, the [O/Fe] value was obtained by adopting IRFM temperatures, trigonometric gravities, and metallicities from Fe II lines (see discussions in Thévenin & Idiart 1999; AGP01).

The list of atomic lines present in the H band compiled by Meléndez & Barbuy (1999) and Meléndez (1999) was adopted, together with molecular lines of CN $A^2\Pi$ - $X^2\Sigma$, CO $X^1\Sigma^+$ (Meléndez & Barbuy 1999), and OH ($X^2\Pi$). The IR OH vibration-rotation lines ($X^2\Pi$) used in this work, from the first-overtone ($\Delta v = 2$) sequence, were described in Meléndez et al. (2001). Energy levels for the OH lines were computed from

molecular parameters given in Coxon & Foster (1992) and Abrams et al. (1994). Molecular oscillator strengths were calculated from Einstein coefficients given by Goldman et al. (1998), which are accurate to 10-15%, depending on the molecular quantum numbers, according to the authors.

The list of OH lines used for oxygen abundance determination together with their molecular gf-values, energy levels, and equivalent widths are given in Table 7. The fit of synthetic spectra of OH lines for HD 110184 is shown in Figure 1.

The oxygen abundances derived show a dependence on the carbon abundances adopted. Carbon abundances were derived from the CH $A^2\Pi$-$X^2\Sigma$ G band at $\sim$ 4300 Å, from optical FEROS spectra, for five stars. Details on the atomic and molecular database used are described in Castilho et al. (1999). The observed and synthetic spectra of the G band for HD 110184 are shown in Figure 2. For HD 122956, the 1.56μm CO lines were used to derive its carbon abundance, whereas for HD 134440, the value given in Carbon et al. (1987) was adopted.

The carbon and oxygen abundances derived from IRFM $T_{\rm eff}$, trigonometric gravities, and [Fe II/H] are given in Table 8.

The solar oxygen abundance has been recently revised by Holweger (2001) and Allende Prieto et al. (2001). The main change in the solar oxygen abundance derived from the forbidden line is due to the presence of a Ni I line not considered before, and ϵ(O) = 8.74 was found by Allende Prieto et al. (2001). Holweger (2001) gives ϵ(O) = 8.69 using several permitted lines. Note that the oscillator strength of the [O I] line adopted by Allende Prieto et al. (2001) is log gf = -9.72, 0.03 dex higher than previous values around log gf = -9.75, leading to lower oxygen abundances. Grevesse et al. (1996) reported ϵ(O) = 8.87, whereas Grevesse & Sauval (1998) give ϵ(O) = 8.83. The value from Allende Prieto et al. (2001) is obtained with three-dimensional hydrodynamical model atmospheres, whereas if one-dimensional hydrostatic model atmospheres are used, a value of ϵ(O) = 8.77 is obtained. We adopted ϵ(O) = 8.87, and if ϵ(O) = 8.77 is to be considered, the oxygen abundances will be 0.1 dex higher.

3.5. Errors

The errors due to uncertainties on $T_{\rm eff}$, log g, and v_t are inspected by computing the results for HD 110184. In Table 9 the errors for $\Delta T_{\rm eff}$ = 100 K, Δlog g = 0.5 dex, and Δv_t = 0.5 km s^{-1} are given.

4. Discussion

4.1. Reliability of the IR OH lines

OH is a trace component of oxygen abundances in stellar atmospheres, and its measurement is very susceptible to errors in the adopted temperature structure of model atmospheres (Asplund 2001, 2002; AGP01; Lambert 2002). Using 3D hydrodynamical model atmospheres, AGP01 have demonstrated the extreme sensitivity of molecule formation and derivation of oxygen abundances in metal-poor stars relative to calculations with classical 1D hydrostatic model atmospheres and have shown that the oxygen abundance using the classical models may overestimate the derived oxygen abundance.

According to AGP01, for solar or moderate metallicities ([Fe/H] > -1.0), the temperature remains close to the radiative equilibrium value; however, at lower metallicities, the temperature in the outer layers departs significantly from it (Asplund et al. 1999). Radiative heating occurs due to spectral line absorption of continuum photons coming from deeper layers. In metal-poor stars, adiabatic cooling dominates over radiative heating, and the effects of lower temperatures are first seen at the outermost layers, moving toward deeper layers for the lower metallicities. At log τ_{500nm} $\sim$ -3, the average temperature difference between 3D hydrodynamical and 1D hydrostatic models can reach 1000 K (AGP01).

AGP01 verified that OH lines in the IR, with similar line strengths as the UV lines, suffer from granulation abundance corrections just as severe. In Table 9 we give the equivalent widths (EWs) of the different OH lines measured: there is a clear increase in the oxygen abundance derived with increasing EW, as shown in Figure 3. Given that the lower EW lines are more reliable, according to AGP01, we adopt an oxygen abundance resulting from a mean of the five weaker OH lines. It is interesting to note that the effect is stronger for the

most metal-poor stars.

4.2. Comparison with the literature

In Figure 4 the [O/Fe] versus [Fe/H] obtained from IR OH lines in the present work are plotted.

This result is compared with results from the forbidden doublet of [O I]λ6300.31, λ6363.79 Å lines, which is the most reliable oxygen abundance indicator, given that it is immune to non-LTE effects (Kiselman 2001, 2002; Lambert 2002), and besides neutral oxygen is the dominant species in stellar atmospheres. For this reason, we compare the present results based on IR OH lines with results in the literature obtained from the [O I] lines (e.g. Gratton & Ortolani 1986; Barbuy 1988; Barbuy & Erdelyi-Mendes 1989; Sneden et al. 1991; Spite & Spite 1991; Kraft et al. 1992; Nissen & Edvardsson 1992; Shetrone 1996; Balachandran & Carney 1996; Fulbright & Kraft 1999; Gratton et al. 2000; Westin et al. 2000; Balachandran et al. 2001, 2002; Cayrel et al. 2001; Nissen et al. 2001; Smith et al. 2001; Sneden & Primas 2001, 2002; Cowan et al. 2002). (Note that in Meléndez et al. 2001, we have discussed oxygen abundance results from IR OH lines, as compared to UV OH lines and O I lines, and we defer the reader to that discussion for those comparisons.)

The results from the [O I] line were selected according to their S/Ns, such that only results in which the EW is larger than 5 times the error were considered, and we used Cayrel's (1988) formula for the error on the EW $\delta W_\lambda \approx 1.6(\mathrm{w}\times\delta x)^{1/2}/$-(S/N), where w is the FWHM of a typical spectral line and δx is the pixel size. In Figs. 5a-c we plot [O/Fe] versus [Fe/H] from the references above. In Figure 5a the results from different authors are indicated; for 26 stars, two or more different results are plotted. In Figure 5b giants (log $g < 2.5$, *opencircles*) and dwarfs (log $g > 2.5$, $filledcircles$) are indicated, where the mean of values for the same star are considered, differently from Figure 5a, in which all values reported in the listed references are plotted. In Figure 5c the means of [O/Fe] values, as given in Table 10, are plotted in bins of 0.2 dex in [Fe/H], and the size of the circles represents the number of stars in each bin.

Oxygen abundances from IR OH lines at metallicities [Fe/H] < -2.2 show a trend to higher values, in agreement with chemical evolution models. The behavior is also similar to that shown by Sneden & Primas (2001, 2002) for [O/Sc] vs. [Fe/H]. Finally, it is important to note that mixing along the red giant branch could deplete the oxygen in giants, but the effect should be minor, as studied by Gratton et al. (2000).

5. Conclusions

We obtained high-resolution infrared spectra in the *H* band in order to derive oxygen abundances from IR OH lines. In order to have a homogeneous set of stellar parameters, we carried out detailed analyses using equivalent widths of iron lines measured on high-resolution spectra from the FEROS spectrograph at ESO.

1. The sample stars with metallicities [Fe/H] < -2.2 show a slight increase in [O/Fe], with respect to the results for higher metallicity stars. A mean of [O/Fe] = 0.5 is found, similar to the value derived from the forbidden [OI] lines.

2. A clear increase in the oxygen abundance derived with increasing equivalent width is found, such that the stronger lines give higher abundances. We adopt an oxygen abundance resulting from a mean of the weaker OH lines. It is also important to note that the effect is more pronounced for the most metal-poor stars.

3. It is clear that oxygen abundance determinations for the more metal-poor stars derived from very high S/N forbidden [O I] and IR OH lines are needed, as well as 3D model atmospheres calculations, in the case of IR OH lines.

We acknowledge partial financial support from FAPESP and CNPq. J.M. acknowledges the FAPESP postdoctoral fellowship 01/01134-3. We have made use of data from the *Hipparcos* astrometric mission of the ESA. This research is based on observations obtained by staff of the Gemini Observatory, which is operated by the Association of Universities for Research in Astronomy, Inc., under a cooperative agreement with the NSF

on behalf of the Gemini partnership: The National Science Foundation (United States), the Particle Physics and Astronomy Research Council (United Kingdom), the National Research Council (Canada), CONICYT (Chile), the Australian Research Council (Australia), CNPq (Brazil), and CONYCET (Argentina). The IR data presented herein were obtained at the W.M. Keck Observatory, which is operated as a scientific partnership among the California Institute of Technology, the University of California, and the National Aeronautics and Space Administration. The observatory was made possible by the generous financial support of the W.M. Keck Foundation. The FEROS observations at the European Southern Observatory (ESO) were carried out within the Observatório Nacional ON/ESO and ON/IAG agreements, under Fapesp project 1998/10138-8.

REFERENCES

Abrams, M. C., Davis, S. P., Rao, M. L. P., Engleman, R., Jr., Brault, J. W. 1994, ApJS, 93, 351

Allende Prieto, C., García-López, R., Lambert, D.L. & Gustafsson, B. 1999, ApJ, 527, 879

Allende Prieto, C., Lambert, D.L., Asplund, M. 2001, ApJ, 556, L63

Alonso, A., Arribas, S. & Martínez-Roger, C. 1994, A&AS, 107, 365

Alonso, A., Arribas, S. & Martínez-Roger, C. 1996a, A&A, 313, 873

Alonso, A., Arribas, S. & Martínez-Roger, C. 1996b, A&AS, 117, 227

Alonso, A., Arribas, S. & Martínez-Roger, C. 1998, A&AS, 131, 209

Alonso, A., Arribas, S. & Martínez-Roger, C. 1999a, A&AS, 140, 261 (AAM99a)

Alonso, A., Arribas, S. & Martínez-Roger, C. 1999b, A&AS, 139, 335 (AAM99b)

Anthony-Twarog, B. J. & Twarog, B. A. 1994, 107, 1577

Arenou, F., Grenon, M. & Gomez, A. 1992, A&A, 258, 104

Asplund, M. 2001, NARv, 45, 565

Asplund, M. 2002, Joint Discussion 8, Highlights of Astronomy, ASP, in press

Asplund, M., Nordlund, Å., Trampedach, R., Stein, R.F. 1999, A&A, 346, L17

Asplund, M., & García-Pérez, A.E. 2001, A&A, 372, 601 (AGP01)

Balachandran, S. C., Carr, J. S. & Carney, B. W., 2001, NARv, 45, 529

Balachandran, S. C., Carr, J. S. & Carney, B. W., 2002, Joint Discussion 8, Highlights of Astronomy, ASP, in press

Balachandran, S. C. & Carney, B. W. 1996, AJ 111, 946

Barbuy, B. 1988, A&A, 191, 121

Barbuy, B. & Erdelyi-Mendes, M. 1989, A&A, 214, 239

Bell, R. A., Eriksson, K., Gustafsson, B. & Nordlund, A. 1976, A&AS, 23, 37

Bessell, M. S. 1979, PASP, 91, 589

Bessell, M. S. & Brett, J. M. 1988, PASP, 100, 1134

Biémont, E., Baudoux, M., Kurucz, R.L., Ansbacher, W., Pinnington, A.E., 1991, A&A, 240, 539

Burris, D. L., Pilachowski, C. A., Armandroff, T. E. et al. 2000, ApJ, 544, 302

Burstein, D. & Heiles, C. 1982, AJ, 87, 1165

Carbon, D. F., Barbuy, B., Kraft, R. P., Friel, E. D., & Suntzeff, N. B. 1987, PASP, 99, 335

Castilho, B.V., Spite, F., Barbuy, B., Spite, M., De Medeiros, J.R., Gregorio-Hetem, J. 1999, A&A, 345, 249

Cavallo, R. M., Pilachowski, C. A., Rebolo, R. 1997, PASP, 109, 226

Cayrel, R. 1988, IAU Symp. 132, eds. R. Cayrel, G. Cayrel de Strobel, M. Spite, (Dordrecht: Kluwer), 354

Cayrel, R., Perrin, M.-N., Barbuy, B. & Buser, R. 1991, A&A, 247, 108

Cayrel, R., Anderson, J., Barbuy, B. et al. 2001, NARv, 45, 533

Cowan, J.J., Sneden, C., Burles, S., et al. 2002, ApJ, in press

Coxon, J. A. & Foster, S. C., 1992, Can. J. Phys., 60, 41

François, P. 1996, A&A, 313, 229

François, P., Spite, M., & Spite, F. 1993, A&A, 274, 821

Fuhr, J. R., Martin, G. A. & Wiese, W. L. 1988, J. Phys. Chem. Ref. Data 17, Suppl. 4

Fulbright, J. P. 2000, AJ, 120, 1841

Fulbright, J. P. & Kraft, R. P. 1999, AJ, 118, 527

Goldman, A., Shoenfeld, W. G., Goorvitch, D., Chackerian C. Jr., Dothe, H., Mélen, F., Abrams, M. C., Selby, J. E. A. 1998, JQSRT, 59, 453

Gratton, R. G., & Sneden, C. 1991, A&A, 241, 501

Gratton, R. G., & Sneden, C. 1994, A&A, 287, 927

Gratton, R. G., Sneden, C., Carretta, E. & Bragaglia, A. 2000, A&A, 354, 169

Gratton, R. G. & Ortolani, S. 1986, A&A, 169, 201

Grevesse, N., Noels, A. & Sauval, J. 1996, in ASP Conf. Ser. 99, eds. S.S. Holt, G. Sonneborn, p. 117

Grevesse, N. & Sauval, A.J., 1998, SSRv, 85, 161

Guo, B., Ansbacher, W., Pinnington, E.H. et al. 1992, Phys. Rev. A46, 641

Gustafsson, B., Bell, R. A., Eriksson, K. & Nordlund, Å. 1975, A&A, 42, 407

Hakkila, J., Myers, J. M., Stidham, B., & Hartmann, D. H. 1997, AJ, 114, 2043

Hannaford, P., Lowe, R.M., Grevesse, N., Noels, A. 1992, A&A, 259, 301

Hauck, B. & Mermilliod, M. 1998, A&AS, 129, 431

Heise, C., Kock, M. 1990, A&A, 230, 244

Hinkle, K., Lambert, D.L. 1975, MNRAS, 170, 447

Hinkle, K., Wallace, L., Livingston, W. 1995, *Infrared Atlas of the Arcturus Spectrum, 0.9-5.3 μm*, KPNO/NOAO

Holweger, H. 2001, in Solar and Galactic Composition, ed. R.F. Wimmer-Schweingruber, AIP Conf. Proc. 598, 23

Kaufer, A., Stahl, O., Tubbesing, S. et al. 2000, Proc. SPIE, 4008, 459

King, J. R. 1997, PASP, 109, 776

Kiselman, D. 2001, NARv, 45, 559

Kiselman, D. 2002, Joint Discussion 8, Highlights of Astronomy, ASP, in press

Kraft, R. P., Sneden, C., Langer, G. E. & Prosser, C. F. 1992, AJ, 104, 645

Kroll, S., Kock, M. 1987, A&AS, 67, 225

Lambert, D. L. 2002, Joint Discussion 8, Highlights of Astronomy, ASP, in press

Livingston, W., Wallace, L. 1991, *An Atlas of the Solar Spectrum in the Infrared from 1850 to 9000 cm^{-1}, 1.1-5.4 μm*, KPNO/NOAO

McLean, I. S., Becklin, E. E., Bendiksen, O. et al. 1998, SPIE, 3354, 566

McWilliam A., Preston, G. W., Sneden, C., & Searle, L. 1995, AJ, 109, 2757

Meléndez, J. 1999, MNRAS, 307, 197

Meléndez, J. & Barbuy, B. 1999, ApJS, 124, 527

Meléndez, J., Barbuy, B. & Spite, F. 2001, ApJ, 556, 858

Mermilliod, J.-C., Mermilliod, M. & Hauck, B. 1997, A&AS, 124, 349

Nave, G., Johansson, S., Learner, R.C.M. et al. 1994, ApJS, 94, 221

Nissen, P. E., Edvardsson, B. 1992, A&A, 261, 255

Nissen, P. E., Høg, E. & Schuster, W. 1997, in Hipparcos, Venice '97 (ESO SP-402), p. 225

Nissen, P., Primas, F. & Asplund, M. 2001, NARv, 45, 545

Norris, J., Bessell, M.S., & Pickles, A.J. 1985, ApJS, 58, 463

O'Brian, T.R., Wickliffe, M.E., Lawler, J.E. et al., 1991, J. Opt. Soc. Am. B8, 1185

Pauls, U., Grevesse, N., Huber, M.C.E., 1990, A&A, 231, 536

Perryman, M.A.C., Lindegren, L., Kovalevsky, J. et al. 1997, A&A, 323, L49

Peterson, R.C., Kurucz, R.L., Carney, B.W. 1990, ApJ, 350, 173

Pilachowski, C. A., Sneden, C. & Kraft, R. P. 1996, 111, 1689

Ryan, S. G. & Deliyannis, C. P. 1998, ApJ, 500, 398

Schnabel R., Kock, M., Holweger, H. 1999, A&A, 342, 610

Schnabel R., & Kock, M. 2001, Phys. Rev. A, 63, 2519

Shetrone, M. D. 1996, AJ, 112, 1517

Smith, V.V., Cunha, K., King, J.R. 2001, AJ, 122, 370

Sneden, C., Kraft, R. P., Prosser, C. F. & Langer, G. E. 1991, AJ 102, 2001

Sneden, C. & Primas, F. 2001, NARv, 45, 513

Sneden, C. & Primas, F. 2002, Joint Discussion 8, Highlights of Astronomy, ASP, in press

Spiesman, W. J. & Wallerstein, G. 1991, AJ, 102, 1790

Spite, M. & Spite, F. 1991, A&A 252, 689

Thévenin, F., Idiart, T. 1999, ApJ, 521, 753

Tomkin, J. & Lambert, D. L. 1999, ApJ, 523, 234

Westin, J., Sneden, C., Gustafsson, B. & Cowan, J.J. 2000, ApJ, 530, 783

AAS LaTeX macros v5.0.

TABLE 1
LOG OF OBSERVATIONS

Star	V	Date	Exposure (s)	S/N	Wavelength	Telescope
HD 2796	8.50	2001-11-20	12×300	150	1.49-1.75μm	Keck
HD 6268	8.11	2000-12-15	12×100	450	1.49-1.75μm	Keck
BD-180271	9.85	2000-12-15	13×200	400	1.49-1.75μm	Keck
HD 110184	8.31	2000-05-20	8×80	180	1.46-1.70μm	Keck
HD 122956	7.22	2000-05-20	6×60	300	1.46-1.70μm	Keck
HD 134440	9.44	2000-05-20	8×150	200	1.46-1.70μm	Keck
BD-185550	9.26	2001-06-12	12×120	350	1.49-1.75μm	Keck
HD 2796	8.50	2001-10-01	2400	240	360-900nm	ESO
HD 6268	8.11	2001-10-01	1800	320	360-900nm	ESO
BD-180271	9.85	2001-10-01	3600	340	360-900nm	ESO
HD 110184	8.31	2001-01-18	1800	300	360-900nm	ESO
BD-185550	9.26	2001-10-01	3600	200	360-900nm	ESO

TABLE 2
COLORS

Star	E(B-V)	$(b-y)_0$	$(V-R)_0^J$	$(J-K)_0^{TCS}$	$(V-K)_0^{TCS}$
HD 2796	0.068	0.538	0.714	0.540	2.212
HD 6268	0.016	0.586	0.770	—-	—-
BD-180271	0.005	0.841	1.026	0.728	3.010
HD 110184	0.0	0.818	0.977	0.702	2.918
HD 122956	0.041	0.638	0.813	—-	2.558
HD 134440	0.0	0.522	0.762	0.586	2.293
BD-185550	0.117	0.599	0.791	0.598	2.389

NOTE.—Subscript J is for Johnson; subscript TCS is for Telescopio Carlos Sánchez

TABLE 3
EFFECTIVE TEMPERATURES (K) BASED ON IRFM (SECT. 3.1)

Star	IRFM calibration (AAM99a)					IRFM AAM99b	IRFM mean
	b-y	V-R	V-K	J-K	mean		
HD 2796	4840	4822	4858	4882	4851	4867	4859
HD 6268	4739	4670	—-	—-	4705	—	4705
BD-180271	4239	4112	4190	4277	4212	4277	4245
HD 110184	4272	4199	4249	4376	4274	4250	4262
HD 122956	4553	4547	4519	—-	4540	—	4540
HD 134440	4850	4638	4709	4669	4717	4746	4732
BD-185550	4789	4637	4679	4682	4697	4668	4683

TABLE 4
GRAVITIES (LOG g)

Star	*Hipparcos*	Evolutionary	Mean (Adopted)
HD 2796	—	1.7	1.7±0.3
HD 6268	—	1.5	1.5±0.3
BD-180271	—	0.7	0.7±0.3
HD 110184	—	0.7	0.7±0.3
HD 122956	1.7±0.3	1.5	1.6±0.3
HD 134440	4.8±0.04	4.8	4.8±0.1
BD-185550	—	1.7	1.7±0.3

TABLE 5
REVISED [O/FE] VALUES FROM OH-IR LINES

Star	$T_{\rm eff}$ IRFM	log $g^{\rm Hip}$	[Fe II/H]	[O/Fe]
HD 2665	4980	2.3	−1.90	0.48
HD 6582	5305	4.5	−0.83	0.26
HD 6755	5030	2.9	−1.56	0.16
HD 21581	4870	2.7	−1.50	0.20
HD 25329	4810	4.8	−1.76	0.53
HD 26297	4320	1.1	−1.64	0.27
HD 29574	4030	0.5	−1.70	0.15
HD 37828	4390	1.6	−1.28	0.43
HD 103095	5035	4.7	−1.27	0.25
HD 165195	4240	0.7	−2.14	0.43
HD 187111	4260	0.7	−1.67	0.51
HD 206739	4650	1.7	−1.52	0.29
HD 216143	4490	1.0	−2.08	0.57
HD 221170	4410	1.1	−2.00	0.21
BD +060648	4220	0.8	−1.89	0.30

TABLE 6
ADOPTED ATMOSPHERIC PARAMETERS AND LITERATURE VALUES

Star	IRFM, log g and Fe II				Literature parameters (mean values)				
	$T_{\rm eff}$ IRFM	log g	[Fe II/H]	v_t	$T_{\rm eff}$	log g	[Fe/H]	v_t	ref.
HD 2796	4860	1.7	−2.26	1.9	4910	1.4	−2.34	2.1	1,2,3,4
HD 6268	4705	1.5	−2.35	1.9	4690	1.3	−2.43	1.9	1,3,4
BD-180271	4245	0.7	−2.35	2.5	4230	0.5	−2.39	1.9	5
HD 110184	4262	0.7	−2.41	2.4	4294	0.5	−2.50	2.1	3,4,6,7
HD 122956	4540	1.6	−1.60	1.6	4631	1.4	−1.75	1.7	3,4,6-11
HD 134440	4732	4.8	−1.44	1.0	4804	4.6	−1.47	1.1	12-15
BD-185550	4683	1.7	−2.87	1.7	4698	1.3	−2.93	2.0	1,3,4,16-17

REFERENCES.—(1) McWilliam et al. 1995; (2) François 1996; (3) Pilachowski et al. 1996; (4) Burris et al. 2000; (5) Shetrone 1996; (6) Sneden et al. 1991; (7) Fulbright 2000; (8) Gratton & Sneden 1991; (9) François, Spite & Spite 1993; (10) Gratton & Sneden 1994; (11) Gratton et al. 2000; (12) Tomkin & Lambert 1999; (13) Ryan & Deliyannis 1998; (14) King 1997; (15) Spiesman & Wallerstein 1991 (16) Cavallo, Pilachowski & Rebolo 1997 (17) Peterson, Kurucz, Carney 1990

TABLE 7
EQUIVALENT WIDTHS (MÅ) OF IR OH LINES

v'-v", branch, J"	λ (Å)	χ_{exc} (eV)	log gf	HD 2796	HD 6268	BD -1802	HD 1101	HD 1229	HD 1344	BD -1855
2-0 P2f 6.5	15002.15	0.134	−5.578	...	...	...	...	19	...	...
2-0 P2e 6.5	15003.12	0.134	−5.578	...	...	...	...	21	...	...
2-0 P1e 7.5	15021.04	0.127	−5.520	...	...	48	51	...	...	...
2-0 P1f 7.5	15022.86	0.128	−5.520	...	...	48	...	...	...	...
2-0 P2f 8.5	15264.61	0.210	−5.429	...	...	44	32	...	...	...
2-0 P2e 8.5	15266.17	0.210	−5.429	...	...	42	31	23	...	7.5
2-0 P1e 9.5	15278.52	0.205	−5.382	...	...	50	40	26	...	8.0
2-0 P1f 9.5	15281.05	0.205	−5.382	...	...	49	39	26	...	6.0
3-1 P2e&f 2.5	15283.62	0.478	−5.312	...	...	26	...	16	...	...
3-1 P2e&f 3.5	15391.14	0.494	−5.137	...	...	36	...	...	...	...
2-0 P2e 9.5	15407.29	0.255	−5.365	...	...	...	...	...	...	4.5
2-0 P2e 9.5	15409.17	0.255	−5.365	...	...	48	...	...	...	4.3
2-0 P1e 10.5	15419.46	0.250	−5.323	...	...	58	...	...	...	7.5
2-0 P1f 10.5	15422.37	0.250	−5.323	...	...	58	...	...	...	8.0
3-1 P1e 5.5	15535.46	0.507	−5.230	...	...	26	18	16	13	5.0
3-1 P1f 5.5	15536.71	0.507	−5.230	...	...	22	16	16	12	5.5
2-0 P2e 10.5	15560.24	0.304	−5.307	...	12	52	35	31	23	7.0
4-2 R2e&f 2.5	15565.91	0.899	−5.003	...	...	16	...	...	10.5	...
2-0 P1e 11.5	15568.78	0.299	−5.269	...	10	47	36	27	25	5.0
2-0 P1f 11.5	15572.08	0.300	−5.269	...	11	52	38	28	29	7.2
3-1 P2f 5.5	15626.70	0.541	−5.198	...	...	...	...	21	...	...
3-1 P2e 5.5	15627.41	0.541	−5.198	...	...	...	...	22	...	...
3-1 P1e 6.5	15651.90	0.534	−5.132	...	...	30	22	...	...	5.5
3-1 P1f 6.5	15653.48	0.534	−5.133	...	...	34	24	...	...	5.5
2-0 P2f 11.5	15717.12	0.357	−5.254	...	...	55	...	...	...	...
2-0 P2e 11.5	15719.70	0.358	−5.254	...	...	52	...	...	...	...
2-0 P1e 12.5	15726.72	0.353	−5.219	7	...	47	...	...	...	...
2-0 P1f 12.5	15730.44	0.354	−5.219	6	...	45	...	...	...	...
2-0 P1f 13.5	15897.70	0.412	−5.172	7	...	51	42	...	40	...
3-1 P1e 8.5	15910.42	0.600	−4.976	...	7.3	50	40	...	...	...
3-1 P1f 8.5	15912.73	0.600	−4.976	...	6.3	47	35	...	30	...
3-1 P2f 8.5	16036.89	0.645	−4.957	...	...	37	...	...	...	...
3-1 P2e 8.5	16038.54	0.645	−4.957	...	...	48	...	...	...	...
2-0 P2f 13.5	16061.70	0.476	−5.159	...	...	43	...	...	...	7.5
2-0 P2e 13.5	16065.06	0.477	−5.159	...	...	40	...	...	...	...
3-1 P2e 9.5	16192.13	0.688	−4.893	6	...	...	32	23	26	5.1
3-1 P1e 10.5	16204.08	0.683	−4.851	...	...	58	...	...	...	...
3-1 P1f 10.5	16207.19	0.683	−4.851	...	...	56	...	...	...	...
2-0 P2f 14.5	16247.88	0.542	−5.115	...	...	40	27	25	24	4.3
2-0 P2e 14.5	16251.66	0.543	−5.115	...	...	44	25	24	25	4.1
2-0 P1e 15.5	16255.02	0.538	−5.087	...	6.6	49	28	...	23	...
2-0 P1f 15.5	16260.16	0.538	−5.087	...	7.0	48	28	26	25	...
4-2 P1e 5.5	16346.19	0.927	−4.938	...	...	13	...	...	...	...
4-2 P1f 5.5	16347.49	0.927	−4.938	...	...	12	...	...	...	...
3-1 P2f 10.5	16352.22	0.735	−4.835	...	6.0	54	...	...	...	4.2
3-1 P2e 10.5	16354.58	0.735	−4.835	...	5.9	51	...	...	...	3.8
3-1 P1f 11.5	16368.13	0.731	−4.797	...	...	46	...	...	...	4.0
2-0 P2e 15.5	16448.06	0.612	−5.075	...	...	...	...	...	29	...
2-0 P1e 16.5	16450.37	0.608	−5.048	...	...	...	...	...	27	...
2-0 P1f 16.5	16456.04	0.609	−5.048	...	...	...	...	25	26	...
4-2 P1f 6.5	16472.82	0.953	−4.840	...	...	...	...	10.5	...	...
3-1 P2e 11.5	16526.25	0.787	−4.782	...	...	36	44	21	29	...
3-1 P1e 12.5	16534.58	0.782	−4.746	...	...	36	50	...	26	4.6
3-1 P1f 12.5	16538.59	0.783	−4.746	...	...	35	42	...	...	...
4-2 P2f 6.5	16581.27	0.989	−4.813	...	...	18	...	...	14	...

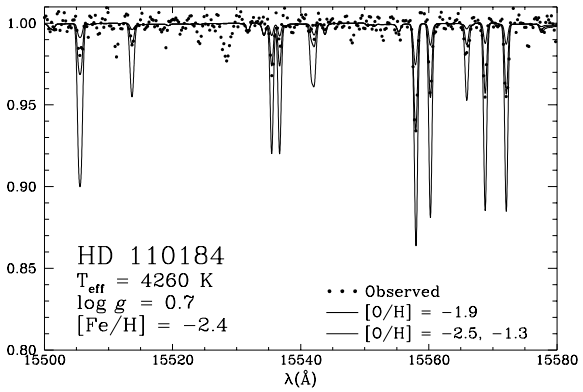

Fig. 1.— Spectrum of HD 110184 (*circles*) compared with synthetic spectra computed with [O/H]: -1.9 (*thick line*) and -2.5 and -1.3 (*thin lines*)

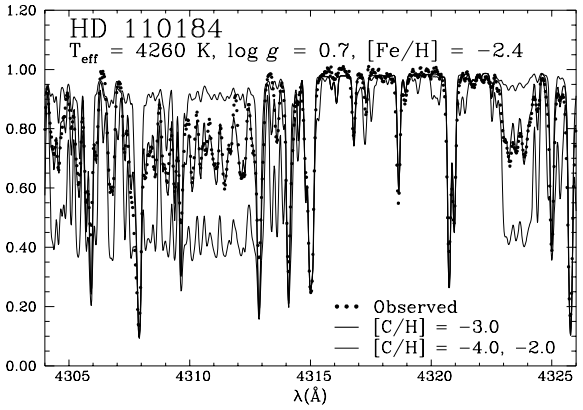

Fig. 2.— Spectrum of HD 110184 (*circles*) compared with synthetic spectra computed with [C/H]: -3.0 (*thick line*) and -4.0 and -2.0 (*thin lines*)

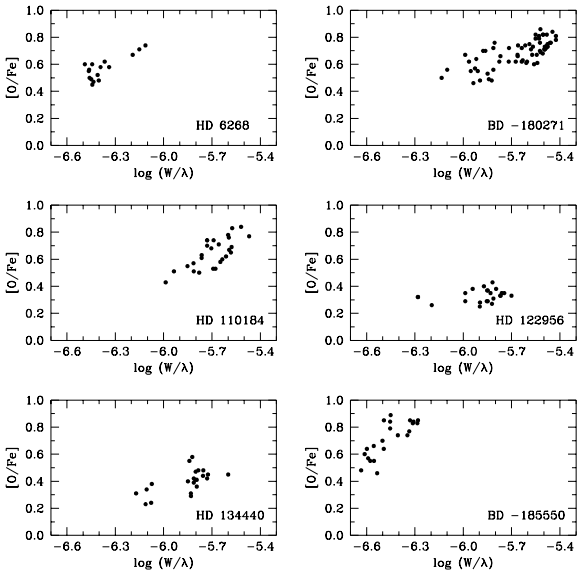

Fig. 3.— [O/Fe] vs. reduced equivalent widths for IR OH lines (see Table 7).

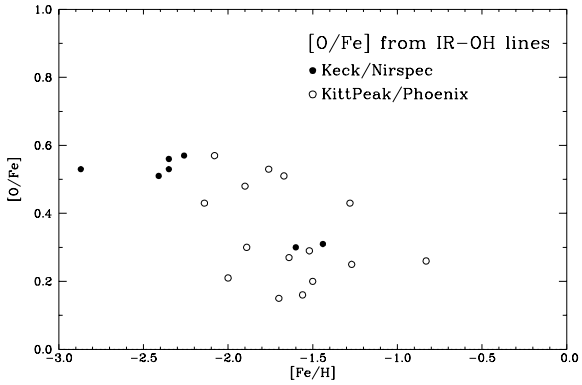

Fig. 4.— [O/Fe] vs. [Fe/H] from IR OH lines. Filled circles show results from the Keck NIRSPEC spectra (this work), and open circles show results from revised Phoenix data (see Meléndez et al. 2001 and Table 5).

TABLE 7—*Continued*

v'-v", branch, J"	λ (Å)	χ_{exc} (eV)	log *gf*	HD 2796	HD 6268	BD -1802	HD 1101	HD 1229	HD 1344	BD -1855
3-1 P1e 13.5	16714.36	0.837	−4.698	...	5.8	47	...	...	...	...
4-2 P1f 8.5	16751.72	1.016	−4.682	...	...	23	...	...	...	...
3-1 P2f 13.5	16895.18	0.901	−4.685	...	...	41	...	...	...	...
3-1 P2e 13.5	16898.78	0.901	−4.685	...	6.0	39	...	...	...	...
4-2 P1e 9.5	16902.73	1.054	−4.616	...	...	26	...	...	...	...
3-1 P1e 14.5	16904.28	0.897	−4.654	...	5.8	26	...	...	...	...
4-2 P1f 9.5	16905.63	1.054	−4.616	...	...	20	...	...	...	...
3-1 P1f 14.5	16909.29	0.898	−4.654	...	...	37	...	24	...	...
4-2 P1e 10.5	17066.13	1.095	−4.556	...	...	21	...	...	...	...
4-2 P1f 10.5	17069.48	1.096	−4.556	...	...	19	...	...	...	...
3-1 P1e 15.5	17104.72	0.960	−4.613	...	5.9	...	...	...	...	...
3-1 P2f 15.5	17308.44	1.031	−4.600	...	...	20	...	...	...	...
3-1 P2e 15.5	17312.99	1.032	−4.600	...	...	22	...	...	...	...

TABLE 8
IRON, CARBON, AND OXYGEN ABUNDANCES

Star	[Fe II/H]	[C/Fe II]	[O/Fe II]
HD 2796	−2.26	−1.00	+0.57
HD 6268	−2.35	−1.13	+0.53
BD-180271	−2.35	−0.73	+0.56
HD 110184	−2.41	−0.58	+0.51
HD 122956	−1.60	−0.50[a]	+0.30
HD 134440	−1.44	+0.19[b]	+0.31
BD-185550	−2.87	−0.39	+0.53

NOTE.—(a) From 1.56 μm CO lines; (b) Adopted from Carbon et al. 1987

Table 9

Sensitivity to T_{eff} , log g and v_t for HD 110184

Abundance	Δ T_{eff} +100 K	Δ log g +0.5 dex	Δv_t +0.5 km s^{-1}	$(\Sigma x^2)^{1/2}$
[FeI/H]	+0.15	-0.18	−0.09	0.25
[FeII/H]	−0.04	+0.13	−0.06	0.15
[O/H]	+0.22	−0.24	+0.04	0.33
[O/FeI]	+0.07	−0.06	+0.13	0.16
[O/FeII]	+0.26	−0.37	+0.10	0.46

Table 10

Mean [O/Fe] from [O I] in bins of 0.2 dex in [Fe/H]

[Fe/H]	[O/Fe]	σ	σ_{mean}	Stars
0.0	−0.04	0.13	0.04	11
−0.2	0.06	0.07	0.02	11
−0.4	0.12	0.08	0.02	16
−0.6	0.19	0.09	0.02	13
−0.8	0.23	0.13	0.03	14
−1.0	0.25	0.14	0.07	4
−1.2	0.33	0.10	0.03	12
−1.4	0.37	0.08	0.02	15
−1.6	0.36	0.10	0.02	19
−1.8	0.34	0.12	0.03	14
−2.0	0.37	0.10	0.04	5
−2.2	0.42	0.13	0.05	7
−2.4	0.40	0.08	0.03	7
−2.6	0.47	0.18	0.08	5
−2.8	0.53	0.04	0.03	2
−3.0	0.66	–	–	1

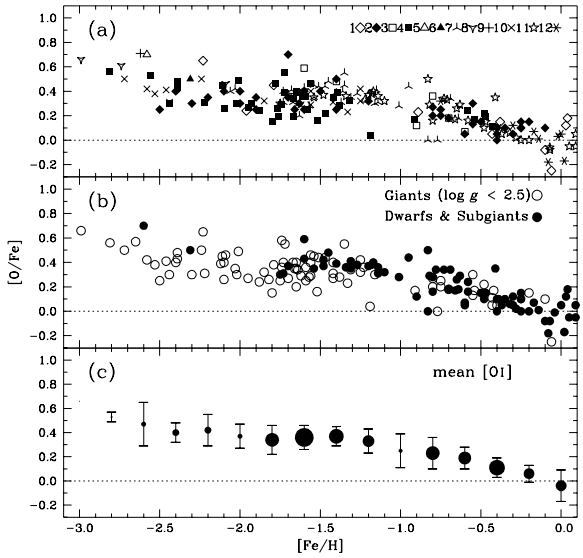

Fig. 5.— [O/Fe] vs. [Fe/H] from [O I] lines. *Top*: Results from (1) Gratton & Ortolani 1986; (2) Barbuy 1988, Barbuy & Erdelyi-Mendes 1989; (3) Spite & Spite 1991; (4) Sneden et al. 1991, Kraft et al. 1992, Shetrone 1996; (5) Balachandran & Carney 1996, Balachandran et al. 2001; (6) Fulbright & Kraft 1999; (7) Gratton et al. 2000; (8) Westin et al. 2000; Cowan et al. 2002; (9) Cayrel et al. 2001; (10) Sneden & Primas 2001; (11) Nissen et al. 2001, Nissen & Edvardsson 1992; (12) Smith et al. 2001. *Middle*: Giants (*open circles*), log $g < 2.5$; Dwarfs and subgiants (*filled circles*), log $g \geq 2.5$. *Bottom*: Mean values and σ from Table 10; the size of the circles represents the number of stars in each bin of 0.2 dex in [Fe/H].